Performance-advantaged ether diesel bioblendstock production by a priori design

Nabila A. Huq[a], Xiangchen Huo[a], Glenn R. Hafenstine[a], Stephen M. Tifft[a], Jim Stunkel[a], Earl D. Christensen[a], Gina M. Fioroni[a], Lisa Fouts[a], Robert L. McCormick[a], Patrick A. Cherry[b], Charles S. McEnally[b], Lisa D. Pfefferle[b], Matthew R. Wiatrowski[a], P. Thathiana Benavides[c], Mary J. Biddy[a], Raynella M. Connatser[d], Michael D. Kass[d], Teresa L. Alleman[a], Peter C. St. John[a], Seonah Kim[a], and Derek R. Vardon[a,1]

[a]National Bioenergy Center, National Renewable Energy Laboratory, Golden, CO 80401; [b]Chemical and Environmental Engineering, Yale University, New Haven, CT 06520; [c]Energy Systems Division, Argonne National Laboratory, Argonne, IL 60439; and [d]Energy & Transportation Science Division, Oak Ridge National Laboratory, Oak Ridge, TN 37831

Edited by Alexis T. Bell, University of California, Berkeley, CA, and approved November 5, 2019 (received for review June 28, 2019)

Lignocellulosic biomass offers a renewable carbon source which can be anaerobically digested to produce short-chain carboxylic acids. Here, we assess fuel properties of oxygenates accessible from catalytic upgrading of these acids a priori for their potential to serve as diesel bioblendstocks. Ethers derived from C_2 and C_4 carboxylic acids are identified as advantaged fuel candidates with significantly improved ignition quality (>56% cetane number increase) and reduced sooting (>86% yield sooting index reduction) when compared to commercial petrodiesel. The prescreening process informed conversion pathway selection toward a C_{11} branched ether, 4-butoxyheptane, which showed promise for fuel performance and health- and safety-related attributes. A continuous, solvent-free production process was then developed using metal oxide acidic catalysts to provide improved thermal stability, water tolerance, and yields. Liter-scale production of 4-butoxyheptane enabled fuel property testing to confirm predicted fuel properties, while incorporation into petrodiesel at 20 vol % demonstrated 10% improvement in ignition quality and 20% reduction in intrinsic sooting tendency. Storage stability of the pure bioblendstock and 20 vol % blend was confirmed with a common fuel antioxidant, as was compatibility with elastomeric components within existing engine and fueling infrastructure. Technoeconomic analysis of the conversion process identified major cost drivers to guide further research and development. Life-cycle analysis determined the potential to reduce greenhouse gas emissions by 50 to 271% relative to petrodiesel, depending on treatment of coproducts.

biooxygenate | biofuel | solvent-free | technoeconomic analysis | life-cycle analysis

There is an increasing need to replace fossil fuels with renewable carbon, particularly for diesel as the demand for medium- and heavy-duty vehicles grows despite electrification (1–3). Oxygenate blendstocks derived from biomass can provide advantaged diesel properties compared to hydrocarbons, often serving to reduce CO, CO_2, and NO_x production (4). Traditional fatty-acid methyl ester (FAME) biodiesel is derived from fats and vegetable oils—feedstocks that are not available at the scale of lignocellulosic biomass. FAME biodiesel has been shown to reduce emissions and increase ignition quality relative to petrodiesel (5) and exhibits only slightly lower energy density than petrodiesel, but presents blending limitations due to its high cloud point and other property differences from conventional diesel (6). However, many bioderived oxygenate blendstocks present even greater challenges from a fuel property standpoint. For example, blending ethanol and other short-chain alcohols into diesel can require emulsifying additives, significantly reduce energy density, and reduce flash point into an unsafe range for fuel handling and storage (7).

The exploration of ethers as diesel candidates is more recent, with recognition of the emissions reduction potential in compression ignition engines and advantaged ignition quality. Their novelty necessitates attention to health and safety risks within the diesel fueling infrastructure. For example, recent work has shown that blending diesel with oxymethylene ethers (OMEs) exhibits nonlinear reduction in sooting with a 50% decrease upon 20 vol % blending (8). However, OMEs have low energy density (~20 MJ/kg) and exhibit high water solubility. The wet environment inherent to the diesel distribution system poses the risk of extracting water-soluble oxygenates and contaminating ground water in the event of a leak (9, 10). A number of ethers and acetals have been explored as diesel blendstocks, with some lacking clear production pathways from lignocellulosic biomass (11–15) and others displaying promising fuel properties that require further work to confirm storage stability and polymer compatibility (16). As such, there is need for high-performance

Significance

The development of market-ready biofuels requires advantaged performance, minimal environmental impact, infrastructure compatibility, and economic feasibility. Here, we leverage conventional and emerging fuel property prediction tools to evaluate a priori the merit of a biobased ether. Continuous ether production was achieved through development of a high-yielding catalytic process. Sufficient quantities of ether were produced to demonstrate improved autoignition quality and reduced intrinsic sooting tendency when blended into petrodiesel, while maintaining infrastructure compatibility. Storage stability was also confirmed upon addition of a common fuel antioxidant. Initial process analysis suggests economic viability and reduced greenhouse gas emissions relative to petrodiesel. Collectively, this work provides an exemplary approach for developing advantaged, derisked biofuels that accounts for performance, environmental impact, and production needs.

Author contributions: N.A.H., X.H., G.R.H., J.S., E.D.C., G.M.F., R.L.M., C.S.M., L.D.P., M.R.W., P.T.B., M.J.B., R.M.C., M.D.K., T.L.A., P.C.S.J., S.K., and D.R.V. designed research; N.A.H., X.H., G.R.H., S.M.T., J.S., E.D.C., G.M.F., L.F., P.A.C., M.R.W., P.T.B., M.J.B., R.M.C., M.D.K., T.L.A., P.C.S.J., and S.K. performed research; N.A.H., X.H., G.R.H., S.M.T., J.S., E.D.C., G.M.F., L.F., R.L.M., P.A.C., C.S.M., L.D.P., M.R.W., P.T.B., M.J.B., R.M.C., M.D.K., T.L.A., P.C.S.J., S.K., and D.R.V. analyzed data; and N.A.H., X.H., G.R.H., R.L.M., C.S.M., M.R.W., P.T.B., M.D.K., T.L.A., and D.R.V. wrote the paper.

Competing interest statement: N.A.H., X.H., G.R.H., and D.R.V. are inventors on a patent application submitted by the Alliance for Sustainable Energy on methods and materials for the production of ether bioblendstocks (US 62/847,700 filed 14 May 2019).

This article is a PNAS Direct Submission.

[1]To whom correspondence may be addressed. Email: derek.vardon@nrel.gov.

This article contains supporting information online at https://www.pnas.org/lookup/suppl/doi:10.1073/pnas.1911107116/-/DCSupplemental.

First published December 16, 2019.

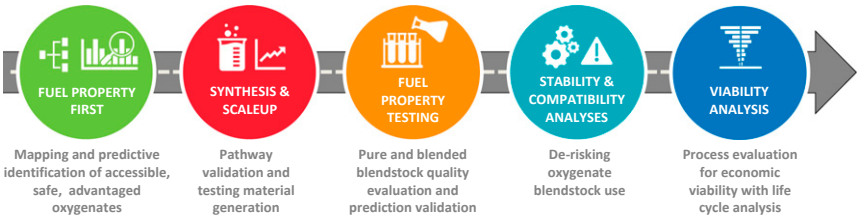

Fig. 1. Process workflow to derisk the production of novel, performance-advantaged oxygenate bioblendstocks for diesel fuel.

ether bioblendstocks which are safe and drop-in-compatible with existing diesel infrastructure.

In this work, we apply a "fuel-property-first" approach to identify advantaged oxygenate diesel blendstocks derived from biomass. Oxygenates are the focus of this work due to their potential advantaged autoignition and sooting properties, as well as retention of oxygen inherent to biomass. In recent work (17), we demonstrated this approach by evaluating hydrocarbon products derived from upgrading lignocellulose-derived anaerobic acids. Specifically, we looked at short-chain (C_2/C_4) carboxylic acids produced from fermentation of lignocellulosic sugars using *Clostridium butyricum* (18). Carboxylic acids, which can be derived from low-cost waste biomass (19, 20), cannot be used directly as fuel due to their corrosive nature and poor fuel properties. However, catalytic upgrading can produce a range of products that span many chemical families (Fig. 1). While synthesis and fuel property testing of each compound is an option to evaluate merit as a diesel blendstock, the diversity of products begs a more efficient and rational approach. By predicting fuel properties of accessible products a priori, we aim to accelerate the development and commercial implementation of high-performance biofuels.

To this end, this work demonstrates an approach to identifying fuel property advantages and derisking the implementation of anaerobic acid-derived ether as a diesel blendstock (Fig. 2). Initially, we computationally screen the fuel properties of target oxygenates to address health- and safety-related aspects such as flash point (T_{flash}) (21, 22), biodegradation potential (23), and toxicity/water solubility (23). Next, we consider fuel performance properties important for market introduction, such as cetane number (CN) (24, 25), boiling point (T_{boil}) or T90, viscosity, and lower heating value (LHV) (26–28). We then evaluate the potential for soot reduction with oxygenated blendstocks. Research has shown that soot emissions are one of the primary contributors to climate change (29) and result in harmful ambient fine

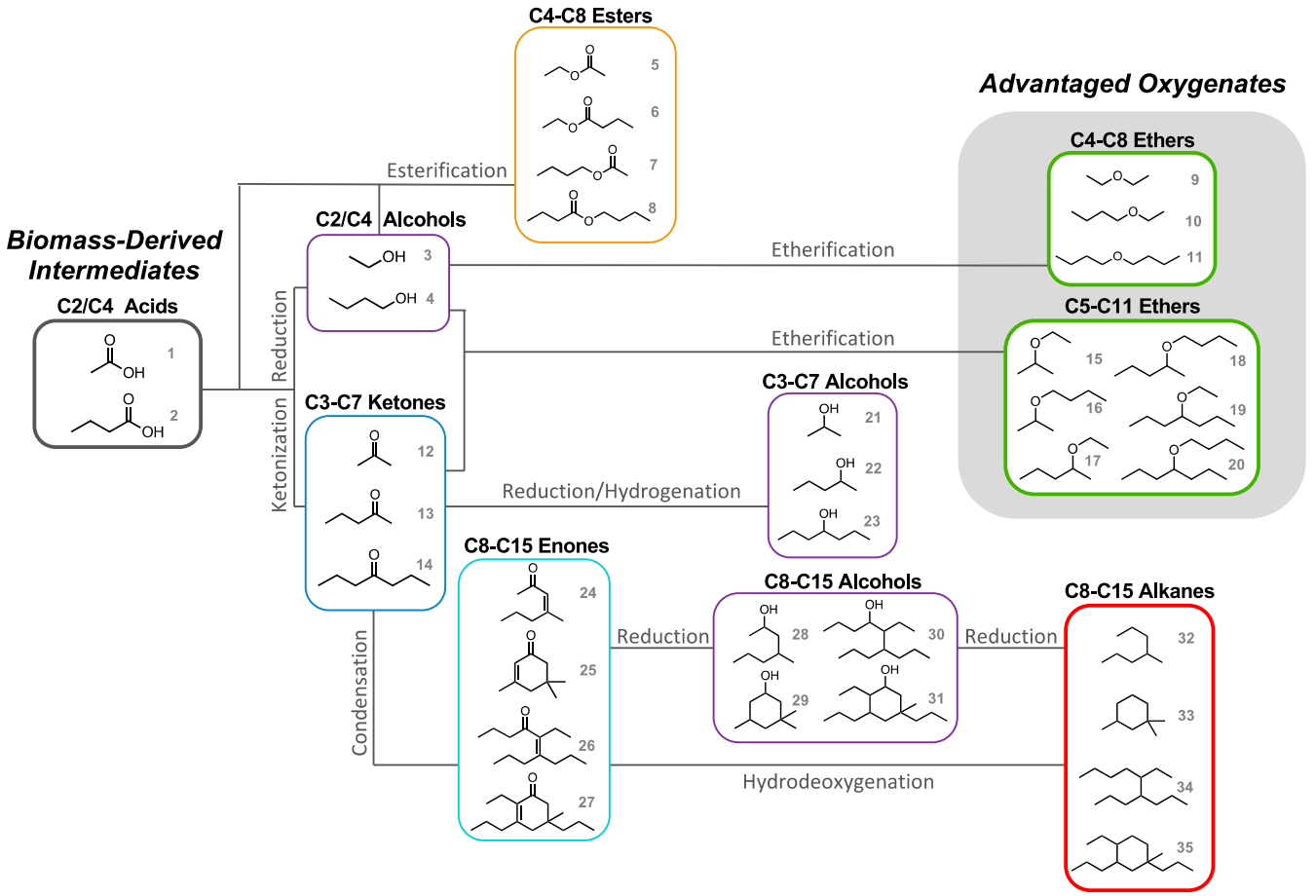

Fig. 2. Conversion pathways and products from the catalytic upgrading of acetic and butyric acid. A subset of products is shown here, numbered for cross-reference (*SI Appendix*, Table S1 and Fig. 3), from the over 50 evaluated chemical species across seven chemical families.

particulates (30). Previous studies have recognized the soot reduction potential of biofuels, but the lack of suitable prediction tools inhibits sooting as a fuel prescreening criterion (31). Yield sooting index (YSI) has been developed to address the need for a laboratory-scale, low-volume sooting tendency metric (32) that provides a good correlation with traditional soot metrics (33). To prescreen oxygenates, we apply a group contribution model to predict YSI as a fuel property criterion (34, 35).

Results from fuel property screening enabled the down-selection to a promising ether diesel bioblendstock candidate. Building on previous work that has recognized the potential merit of bioderived ethers (36, 37), the target compound was synthesized to validate the pathway and compare fuel property measurements against predictions. Continuous solvent-free process conditions were developed to enable liter-scale production, and catalyst design was advanced to improve thermal stability and ether productivity. Compatibility with infrastructure materials and long-term storage stability was then evaluated to derisk deployment. Finally, preliminary technoeconomic and life-cycle analyses were performed in the context of relevant fuel-related metrics, identifying necessary unit operations, and process parameters with significant market and environmental impact.

Results and Discussion

Informed Bioblendstock Selection. Computational tools and predictive models were employed to estimate fuel properties of accessible oxygenate fuel targets derived from anaerobic acids (38). We examined the diversity of compounds accessible from acetic and butyric acid (Fig. 1) to demonstrate the utility of a priori screening for bioblendstock candidates. The conversion pathways were mapped and included carboxylic acid reduction to alcohols (39, 40), carboxylic acid ketonization (41, 42), carboxylic acid and alcohol esterification (43–46), ketone reduction to branched alcohols (47), ketone condensation to enones, followed by enone reduction to alcohols and hydrocarbons (18, 48, 49), alcohol dehydrative etherification (50–53), and ketone and alcohol reductive etherification (37, 54–61). The screened fuel properties included viability from a health and safety perspective, performance characteristics, and deployment feasibility (17, 38).

The advantaged ignition quality (high CN) and minimal sooting potential (low YSI) of ethers derived from C_2/C_4 anaerobic acids was identified using this fuel-property-first approach (17). These favorable characteristics are visualized in Fig. 3, in which the predicted CN and YSI of compounds from Fig. 1 are plotted against the fuel criteria of high cetane (>40, dotted line) and a YSI below that of a surrogate diesel (215, black icon) (38). The high YSI of commercial diesel is a result of the aromatic hydrocarbon content which can range from 20 to 35 vol % (33, 38) with aromatics typically exhibiting YSI values from 100 (benzene) to over 1,000 (62). Ethers consistently fall into the advantaged region, whether produced from dehydrative coupling (compounds **9** to **11**) or from the reductive etherification via ketone and alcohol coupling (compounds **15** to **20**).

Due to challenges with previous oxygenate blendstocks, it was critical to prescreen attributes which may negatively impact health and safety. Water solubility was a concern due to the wet fueling infrastructure of diesel and potential to contaminate drinking water sources. Of the nine down-selected ether compounds, those with carbon numbers 7 or greater were predicted to have water solubility below the 2 g/L limit (Fig. 4*A*) (38). EPI Suite's BIOWIN predictive tools were then used to estimate the potential toxicity and biodegradability in the event of environmental release (23). This technique uses quantitative structural activity responses to estimate the molecule's environmental impact. It predicted most of the structures tend toward biodegradation, with the exception of branched ethers and higher-carbon enones, alcohols, and alkanes (*SI Appendix*, Table S1).

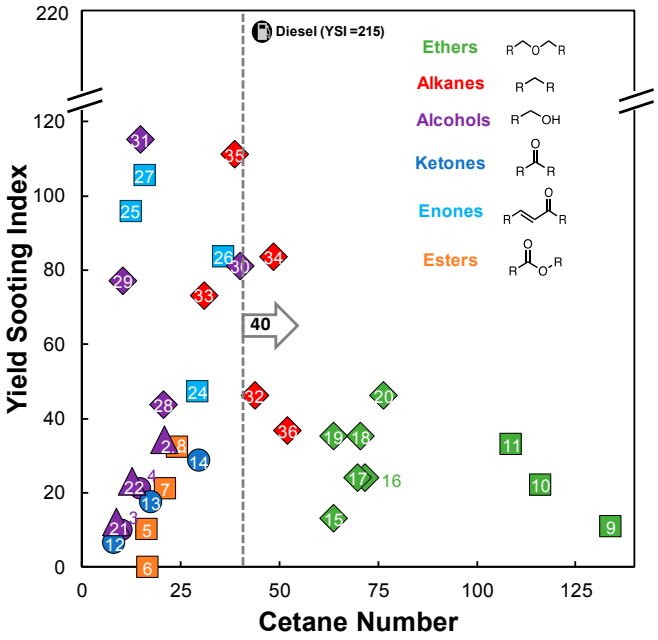

Fig. 3. Predicted CN and YSI fuel properties of mapped molecules, with ethers (green) demonstrating an advantage relative to the other functional groups. Molecule data points are numbered for cross-reference (*SI Appendix*, Table S1 and Fig. 1). The fuel symbol represents measured values for a surrogate diesel (*SI Appendix*, Table S6).

Flash-point criteria, a major safety requirement for fueling, were then evaluated to meet the industry minimum of 52 °C. Flash-point values above the minimum ensure that vapor above the liquid is not ignitable for a given temperature. Flash point does not blend linearly, and even low blend levels can fail specifications. For instance, dibutyl ether (DBE) has a favorable cetane and YSI; however, its flash point of 25 °C is well below the cutoff. The reductive etherification route requires an additional ketonization step compared to dehydrative etherification but provides access to higher-carbon-number, higher-flash-point ethers (Fig. 4*B*). This led to identification of a high-flash-point C_{11} branched ether, 4-butoxyheptane (compound **20**), which was shown to meet diesel fuel property requirements (*SI Appendix*, Table S1, compound **20**). The LHV was comparable (within 10%) to the range of conventional petrodiesel (40 to 46 MJ/kg), to ensure good fuel economy; melting point (cloud point for mixtures) was below 0 °C to facilitate efficacy in cold weather; and the boiling point was below 338 °C to ensure evaporation during combustion (38). Additionally, EPI Suite and EPA TEST analytics (23) show that in the event of an accidental release, 92% of 4-butoxyheptane would partition into the air column and 7.5% would remain in the soil. Although BIOWIN models do not agree on the potential for aerobic degradability (63), it is unlikely that the 4-butoxyheptane will pose environmental risk due to the low predicted water solubility, and therefore mobility (64). This down-selected compound also has low predicted toxicity (acute or chronic) to humans, as well as low anticipated marine impact with nonbioaccumulative properties (23).

Conversion Pathway Development. In order to validate predicted fuel properties for the C_{11} ether, a catalytic pathway was developed with an eye toward scalability (Fig. 5*A*). Vapor-phase hydrogenation of butyric acid to l-butanol has been previously demonstrated in high yield (>98%) using a stable Ru-Sn/ZnO catalyst (39), and vapor-phase butyric acid ketonization to 4-heptanone resulted in complete conversion and high selectivity

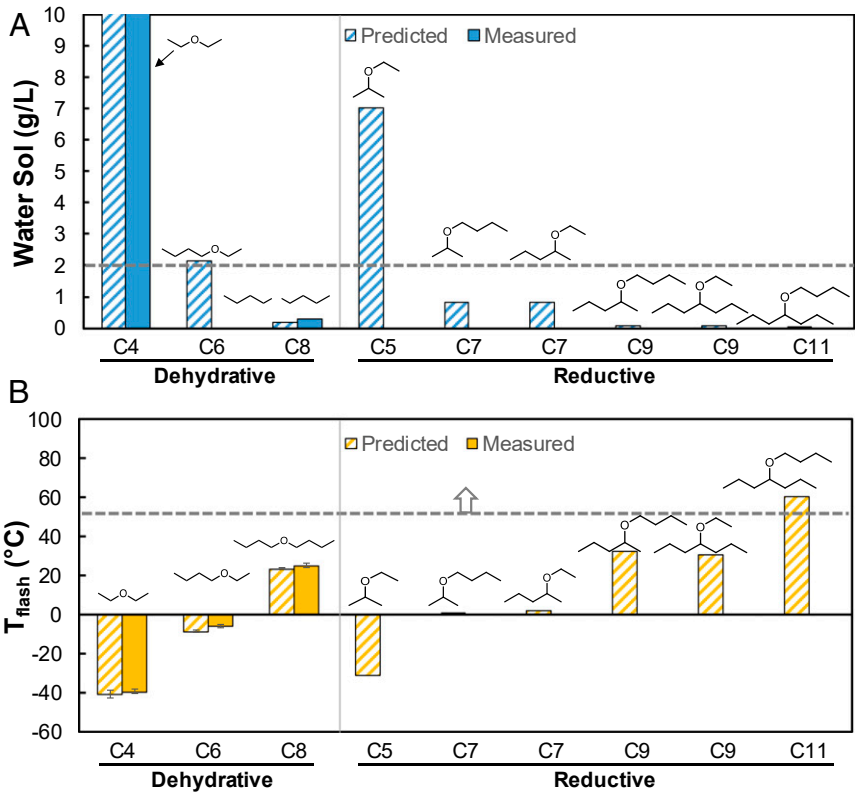

Fig. 4. Ether water solubility and flash point. (*A*) Water solubility limit (<2 g/L) and (*B*) flash-point limit (>52 °C) are shown by dotted lines against ethers produced through dehydrative coupling (*Left*) and reductive etherification (*Right*).

to 4-heptanone (88%) with a commercial ZrO_2 catalyst (17). The reductive etherification pathway developed by Jadhav et al. (37) suggested high yields of branched ethers from ketone and alcohol species in batch reactions. However, our specific target ether, 4-butoxyheptane, was not evaluated and continuous process conditions were not identified.

The reductive etherification reaction between l-butanol and 4-heptanone necessitates the use of a catalyst with acidic and metallic functionality. Previous literature utilized a physical mixture of Amberlyst-15 and 5% Pd/C with acid sites to activate the carbonyl group and Pd metal sites to catalyze the hydrogenolysis of hemiacetal/acetal intermediates or hydrogenation of the enol ether intermediate (37). At a Pd loading of 2.5 mol %, 4:1 molar ratio of l-butanol to 4-heptanone, and a constant H_2 pressure of 10 bar, Jadhav et al. (37) were able to completely convert 2-heptanone to 25 to 50 mg of ether product. Our initial batch reactor screening tests demonstrated conversion of 4-heptanone as high as 87% with ~60% selectivity to the target ether at much lower Pd loading (0.125 mol %) and 1:1 or 2:1 molar reactant equivalents (*SI Appendix*, Figs. S1 and S2). The lower yield of ether relative to 2-heptanone (37) is likely a combination of lower catalyst loading, lack of excess alcohol, and steric hinderance of 4-heptanone.

While feasible, the neat etherification reaction was limited to lower temperatures due to instability of Amberlyst-15 above 120 °C, as is typical for resin acid catalysts which often suffer from aqueous deactivation. To address these shortcomings, two metal oxide acid catalysts were tested that are known to have improved thermal and aqueous stability (65–67). Phosphated niobic acid and zirconia catalysts (Nb_2O_5-PO_4, ZrO_2-PO_4) were synthesized (67) and compared to their nonphosphated metal oxide counterparts. Fig. 5*B* demonstrates the increased temperature and reductive etherification yields with the phosphated version of both catalysts, in addition to retained selectivity at 190 °C. Carbon balance results are provided in *SI Appendix*, Table S2 for all batch tests.

To move toward process relevance, we employed a trickle bed flow reactor to demonstrate continuous ether production. The proposed integrated process for upgrading butyric acid to ether is shown in Fig. 5*C*. Representative time-on-stream data for reductive etherification using Pd/C with Amberlyst-15 are shown in Fig. 5*D*. At a flow rate of 0.20 mL/min (1.1 h^{-1} weight hourly space velocity), over 700 g of target ether was produced (45% mass yield, 70% molar selectivity) with an average 94% mass closure at steady state. No significant carbon was lost to the gas phase. Time-on-stream data reveal the presence of nontarget products including 4-heptanol, heptane, and *n*-butyl ether (Fig. 5*A*), with mass yields provided in *SI Appendix*, Table S3. Multiple continuous-flow reductive etherification runs demonstrated comparable selectivity and activity trends between runs with Amberlyst-15 (*SI Appendix*, Fig. S4). Yields of the target ether and 4-heptanol consistently decreased over time, suggesting catalyst degradation. The Nb_2O_5-PO_4 catalyst was therefore tested under continuous flow conditions (Fig. 5*D*). Improved thermal stability and ether productivity was observed at 190 °C, when compared to Amberlyst-15. The catalyst also showed evidence of regenerability (batch demonstration, *SI Appendix*, Fig. S3), an important consideration for long-term operation. A detailed investigation of catalyst stability, regenerability, and process integration is actively being addressed as the focus of forthcoming work.

Advantaged Bioblendstock Evaluation. Fuel properties of 4-butoxyheptane were then measured to validate model predictions against the screening criteria (Fig. 6 and *SI Appendix*, Table S4). These criteria, as well as the bulk of measured fuel property results, were recently published by Fioroni et al. (38). Barring

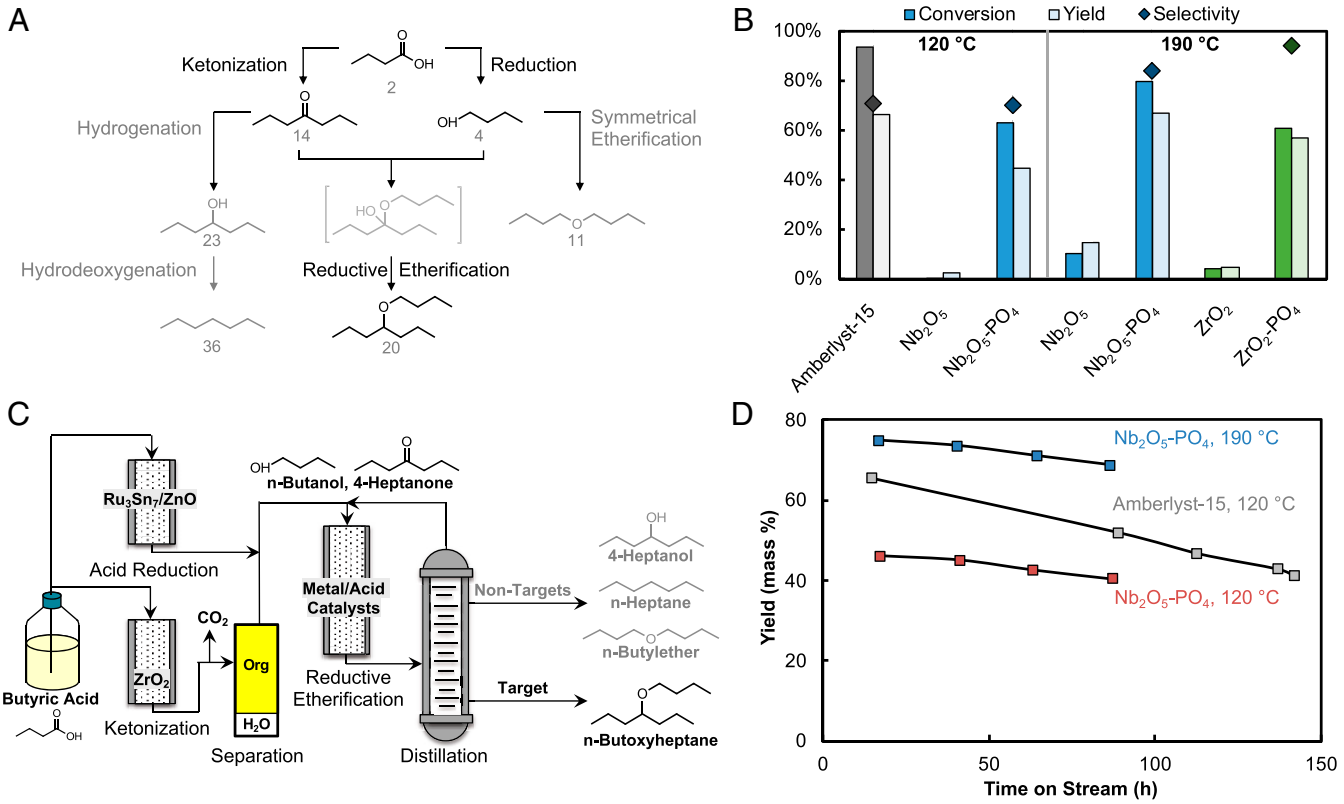

Fig. 5. Catalytic reductive etherification. (*A*) Reaction scheme for target and nontarget compounds. (*B*) Batch reaction tests examining solid acid catalysts. Reaction conditions: 9.9 g of 4-heptanone, 6.4 g of 1-butanol (1:1 molar), 0.23 g Pd/C, and 0.68 g acid catalyst, temperature as indicated, 1,000 pounds per square inch gauge (psig), 5 h, stirred at 800 rpm in 75-mL batch reactor. (*C*) Process scheme for upgrading butyric acid to ether bioblendstock. (*D*) Time-on-stream performance for continuous reductive etherification. Amberlyst-15 reaction conditions: 4-heptanone and 1-butanol (1:1 molar) liquid feed at 0.20 mL/min, 8.8 g catalyst bed (6.6 g acid catalyst and 2.2 g Pd/C), H_2 flow 160 standard cubic centimeters per minute (sccm) at 1,000 psig, 120 °C bed temperature. Runs with Nb_2O_5-PO_4 utilized a reduced catalyst bed loading with in-house-prepared catalyst. Nb_2O_5-PO_4 reaction conditions: 4-heptanone and 1-butanol (1:1 molar) liquid feed at 0.05 mL/min, 2 g catalyst bed (1.5 g acid catalyst and 0.5 g Pd/C), H_2 flow 40 sccm at 1,000 psig, bed temperature as indicated.

melting point (and arguably water solubility), predicted and measured values were comparable for the fuel properties analyzed. The measured melting point was significantly lower than its initial prediction using Joback's group additivity method (68). This inaccuracy is unfortunately common for melting-point estimations; publications typically report root-mean-square errors around 40 °C (69). However, the Joback method's ubiquity in prediction software lends itself to first-pass approximation, and the estimation of −52 °C gave us confidence that the compound would melt below 0 °C. Similarly, the measured water solubility was significantly lower than predicted, with the predicted value well below the 2 g/L limit. A fragmentation-based method which did not require measured property inputs of the molecule was used to estimate water solubility, which is inherently limited by the number of fragments covered by the model. Importantly, the low water solubility of 4-butoxyheptane has favorable implications from a process standpoint. The self-separating organic phase may retain polar compounds and impurities in the aqueous layer, potentially improving ether purity. These metrics, along with a low measured YSI of 58, comprised the preliminary health- and safety-related verifications. Measured fuel performance metrics included LHV and indicated CN (ICN). LHV was within 10% of conventional diesel, meeting the criterion. Remarkably, the measured ICN was 80, double the minimum requirement.

The blendstock was then incorporated into either a base or surrogate diesel fuel to determine if advantaged fuel properties were maintained at 20 vol % blend level (38). Table 1 summarizes the base diesel, blend properties, and fuel property criteria. The cloud point of base diesel favorably decreased upon blending. Boiling point (from thermogravimetric analysis, TGA; *SI Appendix*, Fig. S5) also decreased; however, this change was not large enough to reduce its flash point to below the 52-°C limit. LHV decreased to 40 MJ/kg but remained well above the minimum criterion. For comparison, FAME biodiesel LHVs are typically around 37 MJ/kg and dimethyl ether ∼29 MJ/kg (70, 71). CN (ICN) was slightly improved and observed to blend linearly between 0 and 30 vol % ether (*SI Appendix*, Fig. S6). The blend showed only 4E-6 g/L extraction of the ether into water, indicating low water solubility was maintained. Promisingly, the 20 vol % ether blend significantly reduced YSI of the base diesel from 215 to 173 (20%). This shows the potential of ethers to improve diesel emission properties without sacrificing performance characteristics. Finally, blend viscosity (ν) was determined to be sufficiently low as to not impede spray physics and subsequent fuel utilization and sooting, but not so low as to result in fuel pump leakage (72).

Storage Stability and Material Compatibility. Two distinct characterizations were performed to evaluate the oxidation potential of 4-butoxyheptane during storage. The first utilized a rapid small-scale oxidation test using a PetroOxy instrument to determine induction time, which indicates the potential for fuel to oxidize and degrade. Neat ether was found to have an induction period of 23 min, but upon addition of 100 ppm of a common antioxidant (butylated hydroxytoluene, BHT), it achieved stability above the 60-min requirement for diesel (Table 2) (73). The second experiment evaluated peroxide formation of the blendstock

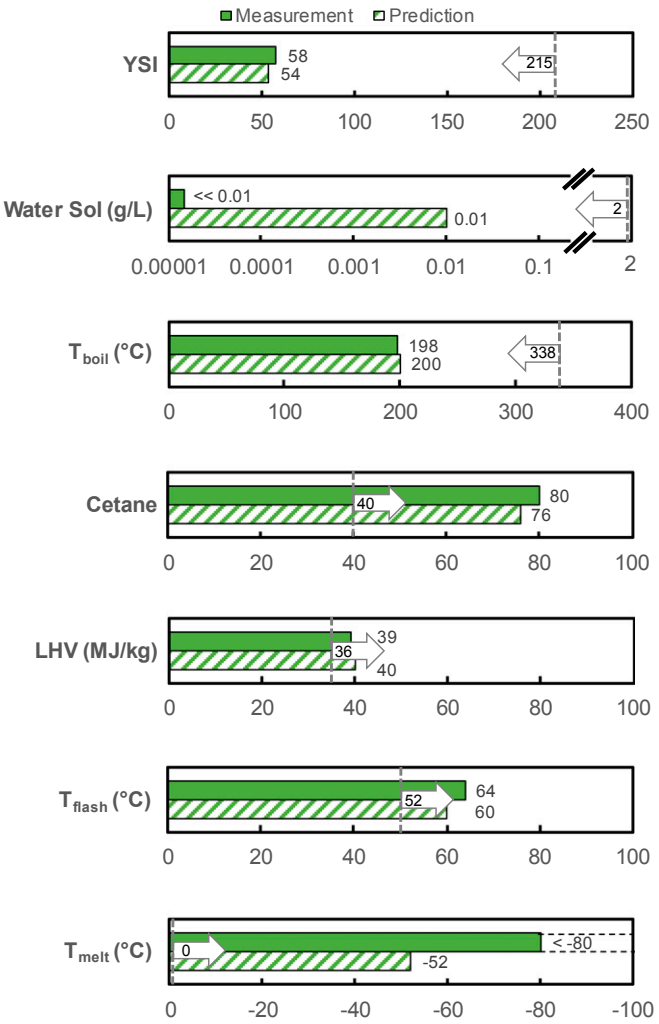

Fig. 6. Fuel property predictions (striped bar) are compared with measured (38) fuel properties where available (solid bar) of the purified C_{11} ether blendstock. The performance-advantaged region for each fuel property is indicated by the arrow marked with the specific numerical criterion for diesel blendstocks. Measured T_{melt} falls below detection limit of the instrument.

during long-term storage (74), which can indicate the potential to form explosive peroxide crystals upon evaporation (*SI Appendix*, Table S7); however, the safety considerations of the organic peroxides formed from this ether have yet to be evaluated. The simulated 6-mo storage experiment (Fig. 7) revealed relative instability of 4-butoxyheptane after 2 mo compared to a baseline isoamyl ether. However, instability of both the blendstock and diesel blend was mitigated by addition of 100 ppm and 20 ppm BHT, respectively. The mechanistic origin of instability will be explored in upcoming work and is likely a result of the low barrier to hydrogen abstraction from the tertiary carbon (C–H bond) next to the oxygen.

Deviating from traditional petrodiesel fuel also introduces the risk of incompatibility with commercial engine and fueling infrastructure components. Especially critical are elastomeric materials used as seals and hoses, listed with applications in *SI Appendix*, Table S8. Hansen solubility analysis (75) predicted a high degree of solubility between the 4-butoxyheptane and base diesel, suggesting potential similarities in swelling effects (*SI Appendix*, Table S9). Predictive polymer solubility parameters and curves (*SI Appendix*, Fig. S7) further suggested polymer–ether compatibility. In order to experimentally verify predictive results, the target blendstock was blended with a certified number 2 diesel (Haltermann Solutions) between 0 and 100 vol %, and then exposed for 4 wk at 21 °C to critical elastomeric engine and fueling components. The volume change after exposure is typically used as the primary means of assessing suitability of a fuel with the fueling component, with large swell indicating some degree of incompatibility (76). Measured volume swell data for the elastomer materials are shown in Fig. 8 after exposure to diesel and 20 vol % blend of 4-butoxyheptane in diesel (full blending results are shown in *SI Appendix*, Fig. S8). Swelling behavior largely agreed with predicted solubility data, and incorporation of 4-butoxyheptane in diesel in almost all cases decreased the swelling on all elastomers. There are two notable cases of the positive effect of ether incorporation. First, it lowered the volume swelling of neoprene to levels to which it becomes potentially tolerable as a static seal (<30% swell); second, it lowered the volume swelling of hydrogenated nitrile butadiene rubbers (HNBR) to that of a potential dynamic seal (<15% swell) (77), where neither application was possible using only diesel. The only exception to this compatibility improvement upon ether incorporation was with silicone exposure, a component which is not commonly found in commercial vehicle fueling infrastructures but occasionally appears in small engine systems. In summary, incorporation of the ether as a diesel blendstock generally decreased volume swell behavior relative to neat diesel and implies potentially improved compatibility with these infrastructure components. While the latter requires confirmation using mechanical testing of exposed elastomers, it indicates the potential for improved component lifetime when blending diesel blending with 4-butoxyheptane.

Economic Feasibility and Life-Cycle Analyses. Finally, major process cost drivers for ether bioblendstock production from lignocellulose-derived butyric acid were evaluated to identify critical areas for future development. A biochemical process model described by Davis et al. (78) was adapted and modified. A block flow diagram of the process is shown in *SI Appendix*, Fig. S10. It is important to note that the analysis assumes n^{th} plant economics, in which several plants using the same process technology have already been built and are operating. This analysis does not claim that the conceptual process design could be implemented in the short

Table 1. Fuel properties of the blendstock blended into a base diesel at 20% by volume are shown against those of the base diesel (38)

Property	Base diesel*	Blend†	Criterion‡
T_{cloud}, °C	−9.7	−11.4	<0
T_{boil}, °C§	333	268	<338
T_{flash}, °C	61	62	>52
LHV, MJ·kg^{-1}	42.9	40	≥36¶
ν at 40 °C, centistokes	*2.66*	*2.12*	1.9–4.1
ICN#	*44.4*	*48.8*	≥40
Water solubility, g/L	Low	Low‖	<2
YSI	*215.1*	*173.1*	Low

The effect of blendstock incorporation on the diesel fuel properties is quantified, shown alongside the minimum fuel criteria. Italics indicate surrogate was used in place of diesel (*SI Appendix*, Table S6).

*See *SI Appendix*, Table S5 for additive-removed diesel properties and *SI Appendix*, Table S6 for surrogate diesel composition and properties.

†Twenty volume percent blend ether in base diesel.

‡All criteria were met by the blend.

§Average of multiple boiling points from TGA of diesel/ether blend (*SI Appendix*, Fig. S5).

¶High LHV criteria of 36 MJ/kg (within 10% of the 40- to 46-MJ/kg range of conventional diesel).

#Twenty percent blend in surrogate diesel (see *SI Appendix*, Fig. S6 for ICN at other blend compositions).

‖A 20 vol % blend of ether in diesel showed 4E-6 g/L extraction of the ether into water, indicating it maintained low water solubility after blending.

Table 2. PetroOxy experiment stability of neat target ether, 100 ppm BHT stabilized ether, and 1,000 ppm BHT stabilized ether

Stabilizer amount, ppm	Stability, min (required: >60 min)
0	23
100	67
1,000	274

term with the specified economics. Details regarding the overall biorefinery model are described in detail elsewhere (78).

The successful implementation of a lignocellulose biochemical conversion process leans heavily on the inclusion of a high-value lignin-derived coproduct (in this case, adipic acid) to overcome high feedstock costs (78) ($78.55 per dry ton) and to reduce greenhouse gas (GHG) emissions (79). An additional coproduct, sodium sulfate, is recovered to partially offset costs for acid and caustic. Adipic acid has an annual global market demand of 2.7 million tons per year (80), while sodium sulfate has an annual demand of over 11.4 million tons per year (81). It is estimated that lignin would be produced at over 60 million tons per year if US mandates are met for second-generation biofuels (82). The impact of this coproduct on the technoeconomic analysis (TEA) can be seen in Fig. 9*A*, which shows lignin utilization contributing a net $3.04 per gasoline gallon equivalent (GGE) credit toward the minimum fuel selling price (MFSP). Similarly, if the lignin fraction of the biomass is not valorized and instead burned for its energy content, the estimated MFSP is $6.79 per GGE. Significant technological barriers must be overcome to economically realize lignin coproducts at commodity scale, with ongoing work to evaluate alternative carbon sources and upstream process configurations to generate carboxylic acids. Additional details on adipic acid production via lignin utilization, including a mass balance of the overall conversion, can be found in Davis et al. (78).

Due to the early stage of this technology and focus on ether diesel blendstock production, upstream unit operations were fixed (e.g., feedstock deconstruction, lignin valorization, biological conversion, and acids separation) to perform a sensitivity analysis on downstream catalytic process parameters and fuel property impacts. Ether conversion parameters were based on current experimental data ("current case") with an output of 31.7 million GGE per year, as well as book-ended with an ideal "best-case" scenario with full selectivity toward the target C_{11} ether and no byproduct formation. Process flow diagrams for the reaction section (all cases) and the separation section (current case) are provided in *SI Appendix*, Fig. S11, with corresponding mass flows for the current case in *SI Appendix*, Table S11. These scenarios provide a theoretical range of the MFSP, as well as insight into the impact of conversion product distributions on MFSP.

The fuel-property-first screening approach was then used to evaluate nontarget etherification products and their suitability in the final blendstock. Predictions and published measurements (Table 3) reveal that the flash points of *n*-heptane (−4 °C) and DBE (25 °C) are below the minimum criterion of 52 °C. Even at low blend levels, low-boiling components can depress flash point of a mixture (83). Therefore, it was critical to ensure economically feasible separation. The CN of 4-hetpanone (20.7) fell below the criterion of 40; however, experimental blending test at low levels (below 30 vol %) suggests no significant impact on the final blendstock (*SI Appendix*, Fig. S6).

Informed by nontarget compound fuel properties, in the current-case analysis, unconverted reactants are recycled, nontarget 4-heptanol is retained in the blendstock, *n*-heptane is utilized as gasoline blendstock based on LHV, and DBE is combusted in a steam boiler. A cost breakdown of the full process is shown in Fig. 9*A*, with C_{11} ether production represented in the "C_4 acid upgrading" category. The downstream catalytic upgrading of butyric acid and subsequent separations accounts for $0.49 per GGE (16.7% of $2.94 per GGE MFSP with lignin valorization). A sensitivity analysis of the full "current case" can be found in *SI Appendix*, Fig. S12, with significant cost drivers identified within the "C_4 acid upgrading" portion.

The impact of catalyst selectivity was also of interest, as a considerable amount of carbon is lost to DBE. In order to evaluate the cost impact, a "DBE-free" scenario was evaluated. The absence of DBE avoided its difficult separation from 4-heptanone, a result of the azeotrope formed at 0.4 mass fraction of DBE. This improved the recovery of 4-heptanone and reduced the "current case" by $0.14. This approaches the "best-case" scenario, which estimates the upper bound of future process and catalyst development. A comparison of relevant cost contributors for the three scenarios can be visualized in Fig. 9*B*, which shows the potential reduction of MFSP from $2.94 per GGE of the "current case" to $2.56 per GGE of the "best case," which is in part due to lower capital and energy requirements for separation, as well as higher carbon utilization and product LHV captured in the "carbon utilization advantage" category (see *SI Appendix*, Table S16 for cost summary of three cases).

Finally, a life-cycle analysis (LCA) of the "current case" was performed to quantify potential reduction in GHG emissions and fossil energy consumption from the ether blendstock production when compared with petrodiesel. The analysis was performed using the GREET 2018 model (84). Since this pathway produces sodium sulfate and adipic acid as coproducts, a system-level allocation methodology was used (85). This methodology distributes the total energy and material contributions to the process and their associated energy and emission burdens to all products by using relative mass output ratios, market values, or energy contents as the allocation basis. Therefore, three allocation methods were used to capture the range of potential reductions: mass-based, market-based, and a hybrid method which distinguishes between energy and nonenergy products. The results of analysis vary greatly depending on the allocation method used to treat these products (85). The results of these analyses can be found in *SI Appendix*, Table S19, showing GHG reductions from processes used for fossil-derived diesel production between 49.8% and 49.2% using mass- and market-based methods, respectively, and 271.3% using the hybrid method. For the latter, the total GHG emissions are −158.7 g CO_2e per MJ of ether/diesel blend produced, which is a significant decrease from the 92.6 g CO_2e per MJ from fossil-derived diesel, due to significant displacement credits from avoided emissions typical of conventional adipic acid and sodium sulfate coproduct production (*SI Appendix*, Table S20). Most of the emissions credits, however, come from the conventional production of adipic acid, which is associated with a high demand of fossil fuel energy (0.13 MJ/g)

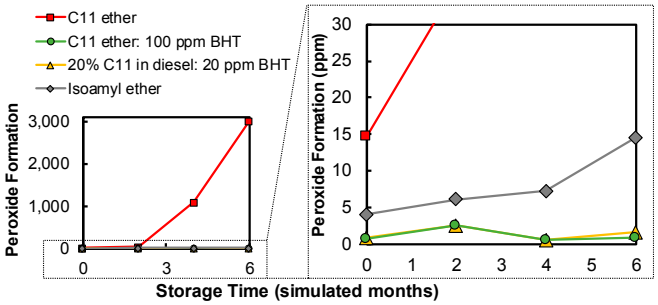

Fig. 7. Simulated 6-mo storage test shows peroxide crystal formation of neat ether and stabilized ether (100 ppm BHT) relative to a baseline isoamyl ether.

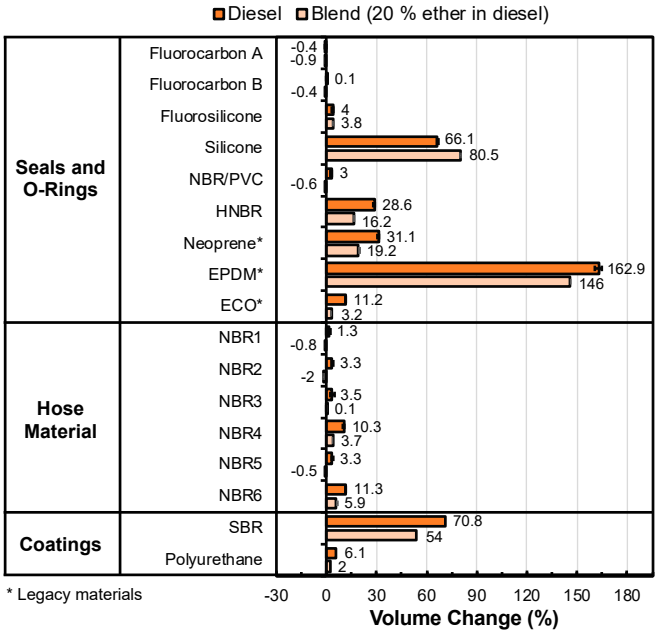

Fig. 8. Volume change results for elastomers exposed to certification diesel (dark orange) and 20 vol % 4-butoxyheptane in diesel (light orange).

and high GHG emissions of about 12 g CO_2e/g, equivalent to 290 g CO_2e/MJ ether/diesel blend. This latter value corresponds to the total credit displaced from production of fossil-derived adipic acid. Similarly, fossil energy consumption was reduced by 49.6% and 49.0% from petrodiesel using mass- and market-based methods, respectively, and 217.1% using the hybrid method. The results also show that the major contributor to the GHG emissions is the electricity input, with around 44% of the total GHG emissions attributed to conversion process energy requirements. Despite this, the LCA indicates the potential for this ether blendstock production process to significantly reduce use of nonrenewable energy relative to conventional processes, as well as greatly reduce GHG emissions.

Future Research Directions. The promising fuel properties of the ether blendstock justify additional research. The current study utilized reagent-grade model compounds, while biomass-derived streams will likely contain impurities such as water, nontarget metabolites, and metals. These impurities will likely impact fuel properties, as well as separation needs. Because impurities and minor components may or may not be acceptable in a finished fuel, the a priori fuel property approach can be applied to inform process specifications, similar to that shown here. Future research with biomass-derived feedstocks will need to identify intermediates that could prevent meeting the fuel performance, health, and safety property criteria presented here, or cause engine operational issues, such as high levels of ash.

Limitations of existing fuel property prediction tools for melting point estimations and water solubility were also made evident over the course of this work. Specifically, predictions based on molecular structure or mechanistic behavior are needed to reach the desired accuracy, rather than predictions based solely on empirical data. For instance, experimental data collected on water solubility and oxidative stability of 4-butoxyheptnae gives cause to explore the mechanistic origins. These predictive needs also extend to assessing properties of mixtures and elucidating blending behaviors that do not track linearly. This is an important addition to extend a priori assessment to include potentially nonselective reactions or purposefully designed blends. The limited predictive capability for novel compounds and complex mixtures also exists in evaluation of toxicity and biodegradability, with accuracy being reliant on availability in data training sets. While full experimental assessment is necessary before deployment, the improved reliability of predictive tools would help reduce uncertainty in the initial downselection of candidate fuels.

When coupled with refined technoeconomic and life-cycle analyses, a fuller picture of process feasibility and fuel performance can emerge for novel oxygenate diesel blendstocks. Cost is a critical component for bioblendstock adoption, and we chose to initially screen blendstocks accessible from low-cost carboxylic acids produced from anaerobic fermentation (78). Alternatively, early-stage cost analysis tools are being developed for biobased processes that rely on high-level correlations based on unit operations and associated capital costs (86, 87). While these tools can enable rapid screening of new conversion routes, integrated mass and energy balance analyses are still needed to deal with more complex unit operations (e.g., separations with recycle) to refine cost and environmental impact assessments.

As identified in our analysis, the production of butyric acid from lignocellulosic biomass remains a major cost barrier requiring lignin valorization to coproducts. Corn stover pretreatment and saccharification represent major process costs, in comparison to downstream bioconversion and catalytic upgrading unit operations. To further reduce feedstock and associated capital costs, ongoing research is evaluating the potential of wet waste for the production of volatile fatty acids compatible with existing anaerobic digestion infrastructure that can undergo a similar catalytic upgrading route (19, 88, 89). Wet waste holds promise due to the large volumes produced, established collection infrastructure, and associated disposal fees that can help offset conversion costs (90). Recent analysis determined that US wet waste provides a potential energy equivalent to displace 18% of US diesel consumption (91).

Ultimately, large enough quantities of bioblendstock will need to be produced to allow for a more rigorous biodegradability and toxicity evaluation, as well as testing in engine combustion and emissions impact studies. As 4-butyoxyheptane is a new chemical,

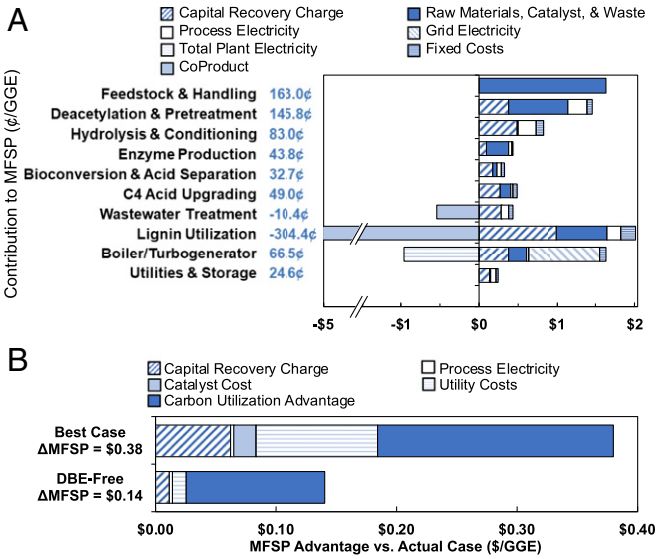

Fig. 9. Ether production technoeconomic analysis. (*A*) Overall process cost breakdown, with net costs shown left of the *y* axis in blue text. Costs relevant to C_{11} ether production are included under "C_4 acid upgrading." (*B*) Cost comparison within the butyric acid conversion and upgrading steps of the "DBE-free" (neglecting DBE formation) and "best case" (100% selectivity to the target) scenarios relative to the experimentally based "current-case" analysis.

Table 3. Selected published and predicted fuel properties of nontarget etherification products for process feasibility analysis

Name	T_{melt} (°C)	T_{boil} (°C)	T_{flash} (°C)	CN	YSI	Water soluble (g/L)
Reactants						
1-butanol	−89.8	118.0	35.0	12.0	22.0	63.2
4-heptanone	−33.0	144.0	48.9	29.6*	28.5	3.2
By-products						
4-heptanol	−41.2	156.0	57.0	20.7	38.5	4.7
n-heptane	−90.6	98.5	−4.0	52.8	36.0	0.003
n-butyl ether	−95.2	140.8	25.0	108.7	38.7	0.30

*Predicted.

future manufacturers may be responsible for ensuring more thorough compliance with various federal requirements (92, 93). Utilization in an engine may point to the need for evaluation of more physically based performance attributes such as fuel spray behavior and mixing, ignition mechanism and kinetics, soot formation mechanisms, and soot properties. This performance testing must be accompanied by work to identify the deployment value of advantaged bioblendstocks for diesel applications, including the impact of reduced sooting and increased CN.

Conclusions

A promising ether diesel blendstock, 4-butoxyheptane, was identified through a predictive fuel-property-first approach to downselect high-potential oxygenate candidates. Fuel property measurements largely agreed with predictive estimations, validating the a priori approach for advantaged diesel blendstock selection. Incorporation of the ether blendstock into diesel demonstrated the favorable effects of enhanced autoignition, low melting point, and decreased sooting tendency. Assessments of safety and compatibility revealed the oxygenate to be low-risk in the context of flammability, toxicity, and storage stability. The development of a solvent-free, continuous catalytic process allowed for high-throughput ether production with improvements in yield and selectivity through catalyst design. Finally, technoeconomic and life-cycle analyses identified process parameters of significant economic and environmental impact that must be realized to reach potential cost and GHG reduction targets.

Materials and Methods

The details behind the materials, experimental methods, and computational methods used in this work can be found in *SI Appendix*, section S1, with additional data available in *SI Appendix*, sections S2 and S3. All data mentioned in the manuscript and *SI Appendix* will be made available to the readers upon request from the corresponding author.

ACKNOWLEDGMENTS. We thank Jon Luecke, J. Hunter Mack, Anne K. Starace, and Jessica L. Olstad for their contributions. A portion of this research was conducted as part of the Co-Optimization of Fuels & Engines (Co-Optima) project sponsored by the US Department of Energy – Office of Energy Efficiency and Renewable Energy, Bioenergy Technologies and Vehicle Technologies Offices. Work at the National Renewable Energy Laboratory was performed under Contract DE347AC36-99GO10337. Part of this work was also supported by Co-Optima through Program Award DE-EE0007983. P.A.C.'s participation was supported by an NSF Research Experiences for Undergraduates supplement to Grant CBET 1604983. The views expressed in the article do not necessarily represent the views of the US Department of Energy or the US Government. The US Government retains and the publisher, by accepting the article for publication, acknowledges that the US Government retains a nonexclusive, paid-up, irrevocable, worldwide license to publish or reproduce the published form of this work, or allow others to do so, for US Government purposes.

1. G. W. Huber, S. Iborra, A. Corma, Synthesis of transportation fuels from biomass: Chemistry, catalysts, and engineering. *Chem. Rev.* **106**, 4044–4098 (2006).
2. S. J. Davis *et al.*, Net-zero emissions energy systems. *Science* **360**, eaas9793 (2018).
3. P. Fairley, Introduction: Next generation biofuels. *Nature* **474**, S2–S5 (2011).
4. D. C. Rakopoulos, C. D. Rakopoulos, E. C. Kakaras, E. G. Giakoumis, Effects of ethanol–diesel fuel blends on the performance and exhaust emissions of heavy duty DI diesel engine. *Energy Convers. Manag.* **49**, 3155–3162 (2008).
5. A. Gopinath, S. Puhan, N. Govindan, Effect of biodiesel structural configuration on its ignition quality. *Int. J. Energy Environ.* **1**, 295–306 (2010).
6. G. Knothe, K. R. Steidley, Kinematic viscosity of biodiesel fuel components and related compounds. Influence of compound structure and comparison to petrodiesel fuel components. *Fuel* **84**, 1059–1065 (2005).
7. B. G. Harvey, W. W. Merriman, R. L. Quintana, Renewable gasoline, solvents, and fuel additives from 2,3-butanediol. *ChemSusChem* **9**, 1814–1819 (2016).
8. A. Damyanov *et al.*, Biogenous ethers: Production and operation in a diesel engine. *Automot. Engine Technol.* **3**, 69–82 (2018).
9. P. J. Squillace, J. F. Pankow, N. E. Korte, J. S. Zogorski, Review of the environmental behavior and fate of methyl tert-butyl ether. *Environ. Toxicol. Chem.* **16**, 1836–1844 (1997).
10. B. S. Sazzad, M. A. Fazal, A. S. M. A. Haseeb, H. H. Masjuki, Retardation of oxidation and material degradation in biodiesel: A review. *RSC Adv.* **6**, 60244–60263 (2016).
11. H. S. Hess, J. Szybist, A. L. Boehman, P. J. A. Tijm, F. J. Waller, "Impact of oxygenated fuel on diesel engine performance and emissions" in *Proceedings of the National Heat Transfer Conference* (American Society of Mechanical Engineers, New York, 2001), pp. 931–941.
12. M. J. Murphy, "Safety and industrial hygiene issues related to the use of oxygenates in diesel fuel" (SAE Tech. Paper 1999-01-1473, Society of Automotive Engineering International, Troy, MI, 1999).
13. İ. Sezer, A review study on the using of diethyl ether in diesel engines: Effects on fuel properties and engine performance. *Energy Technol.* **6**, 2084–2114 (2018).
14. J. Tejero *et al.*, Dehydration of 1-pentanol to di-n-pentyl ether catalyzed by a microporous ion-exchange resin with simultaneous water removal. *Appl. Catal. A Gen.* **308**, 223–230 (2006).
15. L. I. Yeh *et al.*, "Oxygenates: An evaluation of their effects on diesel emissions" (SAE Tech. Paper 2001-01-2019, Society of Automotive Engineering International, Troy, MI, 2001).
16. K. W. Harrison, B. G. Harvey, High cetane renewable diesel fuels prepared from bio-based methyl ketones and diols. *Sustainable Energy Fuels* **2**, 367–371 (2018).
17. X. Huo *et al.*, Tailoring diesel bioblendstock from integrated catalytic upgrading of carboxylic acids: A "fuel property first" approach. *Green Chem.* **21**, 5813–5827 (2019).
18. S. Shylesh *et al.*, Integrated catalytic sequences for catalytic upgrading of bio-derived carboxylic acids to fuels, lubricants and chemical feedstocks. *Sustainable Energy Fuels* **1**, 1805–1809 (2017).
19. W. S. Lee, A. S. M. Chua, H. K. Yeoh, G. C. Ngoh, A review of the production and applications of waste-derived volatile fatty acids. *Chem. Eng. J.* **235**, 83–99 (2014).
20. G. Strazzera, F. Battista, N. H. Garcia, N. Frison, D. Bolzonella, Volatile fatty acids production from food wastes for biorefinery platforms: A review. *J. Environ. Manage.* **226**, 278–288 (2018).
21. R. W. Prugh, Estimation of flash point temperature. *J. Chem. Educ.* **50**, A85 (1973).
22. R. M. Butler, G. M. Cooke, G. G. Lukk, B. G. Jameson, Prediction of flash points of middle distillates. *Ind. Eng. Chem.* **48**, 808–812 (1956).
23. US EPA, Estimation Programs Interface Suite™ for Microsoft® Windows, v 4 (US Environmental Protection Agency, Washington, DC, 2019).
24. T. Kessler, E. R. Sacia, A. T. Bell, J. H. Mack, Artificial neural network based predictions of cetane number for furanic biofuel additives. *Fuel* **206**, 171–179 (2017).
25. M. Dahmen, W. Marquardt, A novel group contribution method for the prediction of the derived cetane number of oxygenated hydrocarbons. *Energy Fuels* **29**, 5781–5801 (2015).
26. W. Boie, Fuel technology calculations. *Energ. Tech.* **3**, 309–316 (1953).
27. W. G. Lloyd, D. A. Davenport, Applying thermodynamics to fossil fuels: Heats of combustion from elemental compositions. *J. Chem. Educ.* **57**, 56 (1980).
28. R. A. Mott, C. E. Spooner, The calorific value of carbon in coal: The dulong relationship. *Fuel* **19**, 226–231, 242–251 (1940).
29. Ö. Gustafsson, V. Ramanathan, Convergence on climate warming by black carbon aerosols. *Proc. Natl. Acad. Sci. U.S.A.* **113**, 4243–4245 (2016).
30. R. Burnett *et al.*, Global estimates of mortality associated with long-term exposure to outdoor fine particulate matter. *Proc. Natl. Acad. Sci. U.S.A.* **115**, 9592–9597 (2018).
31. M. Dahmen, W. Marquardt, Model-based design of tailor-made biofuels. *Energy Fuels* **30**, 1109–1134 (2016).
32. C. S. McEnally, L. D. Pfefferle, Sooting tendencies of oxygenated hydrocarbons in laboratory-scale flames. *Environ. Sci. Technol.* **45**, 2498–2503 (2011).
33. D. Das *et al.*, Sooting tendencies of diesel fuels, jet fuels, and their surrogates in diffusion flames. *Fuel* **197**, 445–458 (2017).
34. D. D. Das, P. C. St. John, C. S. McEnally, S. Kim, L. D. Pfefferle, Measuring and predicting sooting tendencies of oxygenates, alkanes, alkenes, cycloalkanes, and aromatics on a unified scale. *Combust. Flame* **190**, 349–364 (2018).
35. P. C. St. John *et al.*, A quantitative model for the prediction of sooting tendency from molecular structure. *Energy Fuels* **31**, 9983–9990 (2017).
36. N. M. Eagan *et al.*, Catalytic synthesis of distillate-range ethers and olefins from ethanol through Guerbet coupling and etherification. *Green Chem.* **21**, 3300–3318 (2019).
37. D. Jadhav *et al.*, Production of biomass-based automotive lubricants by reductive etherification. *ChemSusChem* **10**, 2527–2533 (2017).
38. G. Fioroni *et al.*, "Screening of potential biomass-derived streams as fuel blendstocks for mixing controlled compression ignition combustion" (SAE Tech. Paper 2019-01-0570, Society of Automotive Engineering International, Troy, MI, 2019).

39. J.-M. Lee *et al*., Direct hydrogenation of biomass-derived butyric acid to n-butanol over a ruthenium-tin bimetallic catalyst. *ChemSusChem* **7**, 2998–3001 (2014).
40. D. R. Vardon *et al*., Ru-Sn/AC for the aqueous-phase reduction of succinic acid to 1,4-butanediol under continuous process conditions. *ACS Catal.* **7**, 6207–6219 (2017).
41. L. Deng, Y. Fu, Q.-X. Guo, Upgraded acidic components of bio-oil through catalytic ketonic condensation. *Energy Fuels* **23**, 564–568 (2009).
42. T. N. Pham, T. Sooknoi, S. P. Crossley, D. E. Resasco, Ketonization of carboxylic acids: Mechanisms, catalysts, and implications for biomass conversion. *ACS Catal.* **3**, 2456–2473 (2013).
43. C.-T. Chen, Y. S. Munot, Direct atom-efficient esterification between carboxylic acids and alcohols catalyzed by amphoteric, water-tolerant TiO(acac)2. *J. Org. Chem.* **70**, 8625–8627 (2005).
44. X. Duan, Y. Liu, Q. Zhao, X. Wang, S. Li, Water-tolerant heteropolyacid on magnetic nanoparticles as efficient catalysts for esterification of free fatty acid. *RSC Adv.* **3**, 13748–13755 (2013).
45. R. Natalino, E. V. V. Varejão, M. J. da Silva, A. L. Cardoso, S. A. Fernandes, p-Sulfonic acid calix[n]arenes: The most active and water tolerant organocatalysts in esterification reactions. *Catal. Sci. Technol.* **4**, 1369–1375 (2014).
46. M. Tao *et al*., Tailoring the synergistic bronsted-lewis acidic effects in heteropolyacid catalysts: Applied in esterification and transesterification reactions. *Sci. Rep.* **5**, 13764 (2015).
47. R. Langer, G. Leitus, Y. Ben-David, D. Milstein, Efficient hydrogenation of ketones catalyzed by an iron pincer complex. *Angew. Chem. Int. Ed. Engl.* **50**, 2120–2124 (2011).
48. M. Balakrishnan *et al*., Novel pathways for fuels and lubricants from biomass optimized using life-cycle greenhouse gas assessment. *Proc. Natl. Acad. Sci. U.S.A.* **112**, 7645–7649 (2015).
49. C. Milone *et al*., Selective hydrogenation of α,β-unsaturated ketone to α,β-unsaturated alcohol on gold-supported iron oxide catalysts: Role of the support. *J. Catal.* **236**, 80–90 (2005).
50. F. Frusteri *et al*., Catalytic etherification of glycerol by tert-butyl alcohol to produce oxygenated additives for diesel fuel. *Appl. Catal. A Gen.* **367**, 77–83 (2009).
51. M. A. Jaworski *et al*., Glycerol etherification with benzyl alcohol over sulfated zirconia catalysts. *Appl. Catal. A Gen.* **505**, 36–43 (2015).
52. J. Rorrer, Y. He, F. D. Toste, A. T. Bell, Mechanism and kinetics of 1-dodecanol etherification over tungstated zirconia. *J. Catal.* **354**, 13–23 (2017).
53. J. Rorrer, S. Pindi, F. D. Toste, A. T. Bell, Effect of alcohol structure on the kinetics of etherification and dehydration over tungstated zirconia. *ChemSusChem* **11**, 3104–3111 (2018).
54. M. Balakrishnan, E. R. Sacia, A. T. Bell, Etherification and reductive etherification of 5-(hydroxymethyl)furfural: 5-(alkoxymethyl)furfurals and 2,5-bis(alkoxymethyl)furans as potential bio-diesel candidates. *Green Chem.* **14**, 1626–1634 (2012).
55. V. Bethmont, F. Fache, M. Lemaire, An alternative catalytic method to the Williamson's synthesis of ethers. *Tetrahedron Lett.* **36**, 4235–4236 (1995).
56. V. Bethmont, C. Montassier, P. Marecot, Ether synthesis from alcohol and aldehyde in the presence of hydrogen and palladium deposited on charcoal. *J. Mol. Catal. A Chem.* **152**, 133–140 (2000).
57. Q. Cui *et al*., Synthesis of ethyl-4-ethoxy pentanoate by reductive etherification of ethyl levulinate in ethanol on Pd/SiO_2 -C catalysts. *ChemSusChem* **11**, 3796–3802 (2018).
58. L. J. Gooßen, C. Linder, Catalytic reductive etherification of ketones with alcohols at ambient hydrogen pressure: A practical, waste-minimized synthesis of dialkyl ethers. *Synlett* **2006**, 3489–3491 (2006).
59. H. Nguyen *et al*., Role of lewis and brønsted acidity in metal chloride catalysis in organic media: Reductive etherification of furanics. *ACS Catal.* **7**, 7363–7370 (2017).
60. M. L. Tulchinsky, J. R. Briggs, One-pot synthesis of alkyl 4-alkoxypentanoates by esterification and reductive etherification of levulinic acid in alcoholic solutions. *ACS Sustain. Chem. Eng.* **4**, 4089–4093 (2016).
61. Y. Wang, Q. Cui, Y. Guan, P. Wu, Facile synthesis of furfuryl ethyl ether in high yield via the reductive etherification of furfural in ethanol over Pd/C under mild conditions. *Green Chem.* **20**, 2110–2117 (2018).
62. C. S. McEnally, D. D. Das, L. D. Pfefferle, Yield Sooting Index Database Volume 2: Sooting tendencies of a wide range of fuel compounds on a unified scale (Harvard Dataverse, ed. V1, 2017).
63. W. Meylan, R. Boethling, D. Aronson, P. Howard, J. Tunkel, Chemical structure-based predictive model for methanogenic anaerobic biodegradation potential. *Environ. Toxicol. Chem.* **26**, 1785–1792 (2007).
64. R. L. McCormick *et al*., "Selection criteria and screening of potential biomass-derived streams as fuel blendstocks for advanced spark-ignition engines" (SAE Tech. Paper 2017-01-0868, Society of Automotive Engineering International, Troy, MI, 2017).
65. A. A. Kiss, A. C. Dimian, G. Rothenberg, Solid acid catalysts for biodiesel production–Towards sustainable energy. *Adv. Synth. Catal.* **348**, 75–81 (2006).
66. T. Okuhara, Water-tolerant solid acid catalysts. *Chem. Rev.* **102**, 3641–3665 (2002).
67. R. M. West, M. H. Tucker, D. J. Braden, J. A. Dumesic, Production of alkanes from biomass derived carbohydrates on bi-functional catalysts employing niobium-based supports. *Catal. Commun.* **10**, 1743–1746 (2009).
68. L. Constantinou, R. Gani, New group contribution method for estimating properties of pure compounds. *AIChE J.* **40**, 1697–1710 (1994).
69. L. D. Hughes, D. S. Palmer, F. Nigsch, J. B. O. Mitchell, Why are some properties more difficult to predict than others? A study of QSPR models of solubility, melting point, and Log P. *J. Chem. Inf. Model.* **48**, 220–232 (2008).
70. P. S. Mehta, K. Anand, Estimation of a lower heating value of vegetable oil and biodiesel fuel. *Energy Fuels* **23**, 3893–3898 (2009).
71. Engineering ToolBox, Fuels–Higher and lower calorific values. https://www.engineeringtoolbox.com/fuels-higher-calorific-values-d_169.html. Accessed 26 June 2019.
72. ASTM International, ASTM D445-18 Standard test method for kinematic viscosity of transparent and opaque liquids (and calculation of dynamic viscosity) (ASTM International, 2018).
73. Top Tier, Diesel performance standard. https://www.toptiergas.com/diesel-performance-specifications/. Accessed 18 September 2019.
74. E. Christensen, R. L. McCormick, Long-term storage stability of biodiesel and biodiesel blends. *Fuel Process. Technol.* **128**, 339–348 (2014).
75. C. M. Hansen, *Hansen Solubility Parameters: A User's Handbook* (CRC Press, Boca Raton, FL, ed. 2, 2007).
76. ASTM International, ASTM D471-16a Standard test method for rubber property—Effect of liquids (ASTM International, 2016).
77. Hannifin, P., Volume change (Parker O-Ring eHandbood, Parker Hannifin O-Ring and Engineered Seals, Lexington, KY, 2018).
78. R. E. Davis *et al*., Process design and economics for the conversion of lignocellulosic biomass to hydrocarbon fuels and coproducts: 2018 biochemical design case update; biochemical deconstruction and conversion of biomass to fuels and products via integrated biorefinery pathways (Tech. Rep. NREL-5100-71949, National Renewable Energy Laboratory, Golden, CO, 2018).
79. A. Corona *et al*., Life cycle assessment of adipic acid production from lignin. *Green Chem.* **20**, 3857–3866 (2018).
80. P. Sriram, B. Merrill, Y. Khan, M. Wu, Adipic acid (IHS Chemical Economics Handbook, IHS Inc., Englewood, CO, 2015).
81. A. Gao, C. Funada, S. Wietlisbach, S. Davis, Sodium sulfate (IHS Chemical Economics Handbook, IHS Inc., Englewood, CO, 2016).
82. M. Langholtz *et al*., Lignin-derived carbon fiber as a co-product of refining cellulosic biomass. *SAE Int. J. Mater. Manuf.* **7**, 115–121 (2014).
83. L. Y. Phoon, A. A. Mustaffa, H. Hashim, R. Mat, A review of flash point prediction models for flammable liquid mixtures. *Ind. Eng. Chem. Res.* **53**, 12553–12565 (2014).
84. Argonne National Laboratory, GREET 2018, Greenhouse gases, regulated emissions and energy use in transportation model (Argonne National Laboratory, Lemont, IL, 2018).
85. H. Cai *et al*., Life-cycle analysis of integrated biorefineries with co-production of biofuels and bio-based chemicals: Co-product handling methods and implications. *Biofuels Bioprod. Biorefin.* **12**, 815–833 (2018).
86. J. T. Claypool, D. R. Raman, Development and validation of a technoeconomic analysis tool for early-stage evaluation of bio-based chemical production processes. *Bioresour. Technol.* **150**, 486–495 (2013).
87. M. Tsagkari, J.-L. Couturier, A. Kokossis, J.-L. Dubois, Early-stage capital cost estimation of biorefinery processes: A comparative study of heuristic techniques. *ChemSusChem* **9**, 2284–2297 (2016).
88. M. Atasoy, I. Owusu-Agyeman, E. Plaza, Z. Cetecioglu, Bio-based volatile fatty acid production and recovery from waste streams: Current status and future challenges. *Bioresour. Technol.* **268**, 773–786 (2018).
89. M. Zhou, B. Yan, J. W. C. Wong, Y. Zhang, Enhanced volatile fatty acids production from anaerobic fermentation of food waste: A mini-review focusing on acidogenic metabolic pathways. *Bioresour. Technol.* **248**, 68–78 (2018).
90. A. Badgett, E. Newes, A. Milbrandt, Economic analysis of wet waste-to-energy resources in the United States. *Energy* **176**, 224–234 (2019).
91. A. Milbrandt, T. Seiple, D. Heimiller, R. Skaggs, A. Coleman, Wet waste-to-energy resources in the United States. *Resour. Conserv. Recycling* **137**, 32–47 (2018).
92. US EPA, Part 79: Registration of fuels and fuel additives. Code of Federal Regulations, Protection of Environment, 18 (Chapter 1 - EPA, Subchapter C, 2018).
93. US EPA, Filing a pre-manufacture notice with EPA. https://www.epa.gov/reviewing-new-chemicals-under-toxic-substances-control-act-tsca/filing-pre-manufacture-notice-epa. Accessed 18 September 2019.